WAVE INTERACTIONS IN LOCALIZING MEDIA — A COIN WITH MANY FACES

J. D. BODYFELT*, T. V. LAPTYEVA*, G. GLIGORIC*,
D. O. KRIMER*,†, Ch. SKOKOS*,‡ and S. FLACH*

*Max-Planck-Institut für Physik Komplexer Systeme,
Nöthnitzer Straße 38, D-01187 Dresden, Germany

†Theoretische Physik, Universität Tübingen,
Auf der Morgenstelle 14, 72076 Tübingen, Germany

‡Center for Research and Applications of Nonlinear Systems,
University of Patras, GR-26500 Patras, Greece

A variety of heterogeneous potentials are capable of localizing linear noninteracting waves. In this work, we review different examples of heterogeneous localizing potentials which were realized in experiments. We then discuss the impact of nonlinearity induced by wave interactions, in particular, its destructive effect on the localizing properties of the heterogeneous potentials.

Keywords: Anderson localization; nonlinearity; delocalization; heterogeneous potential; wave spreading; Wannier–Stark; kicked rotor; Aubry–André.

From communications amongst ourselves to sensing and imaging our surroundings, wave transmissions through media play an integral role in our modern lives. Regardless of their physical origin or scale, most wave systems exhibit phenomena such as scattering, reflection, refraction and interference. This commonality thus provides a framework to discuss universal features. Transmission media, modeled by mathematical potentials, are often idealized with the characteristics of integrability, hermiticity (i.e. closed systems), linearity, and homogeneity. In-situ applications rarely however are at this level of perfection — even in a laboratory, such situations require colossal experimental control and accuracy to achieve. Besides, these small differences from perfection may lead to novel and utilitarian phenomena.

One such small difference is heterogeneity of the medium. This heterogeneity can arise in several different ways, but throughout, attenuation of the wave transmission is possible — a phenomenon called *localization*. The first heterogeneity to be discussed is the presence of randomly distributed impurities, leading to an exponential localization in the eigenstates — called *Anderson localization* (AL). In Sec. 1.1, this AL is described in greater detail. The second form of heterogeneity arises from the presence of a DC-biased electric field, creating an equidistant spectrum and an inverse factorial eigenstate attenuation — called *Wannier–Stark localization*. This case is detailed within Sec. 1.2. The third case, covered in Sec. 1.3, comes from potentials that are arranged in correlated fashions. In these types of heterogeneity, a tuning parameter may allow transitions from localized states to those that are unattenuated, with critical states at the transition point. The last form of heterogeneity to be discussed arises from a specially designed potential, in which localization occurs not spatially, but within a momentum space. This *dynamical localization* will be presented in Sec. 1.4.

In addition to heterogeneity, a second deviation from ideal transmission media is due to wave interaction, resulting in nonlinear dependencies

on wave amplitudes. Examples of such nonlinear potentials are prolific, and include the AC Kerr effect in optical media, atom–atom scattering in boson condensates, screened Coulomb interactions in electrons, and acoustic Langmuir waves in cold plasmas. This nonlinearity can additionally be coupled to heterogeneous localizing potentials, drastically altering the resulting localization. Within Sec. 2, the effect of nonlinearity on the dynamics of packets in localizing media is discussed, with individual subsections corresponding to the four different heterogeneities.

In short, we address what happens when first, the linear waves yield zero conductivity (localized) in heterogeneous media, and then wave interactions are added. Will an insulator change into a conductor, or will localization remain? This is the main question in the interplay between heterogeneity and nonlinearity, and helps define how these two different ingredients collaborate.

1. Linear Waves in Localizing Media

1.1. *Disorder — Anderson localization*

A fundamental problem of condensed matter physics was (and still remains) the study of conductivity of electrons in solids. Since in an infinite perfect crystal, electrons can propagate ballistically, a natural question is raised: what happens in a more realistic situation when there is disorder in the crystal due to impurities or defects? Will the increase of the degree of disorder lead to a decrease of conductivity, or not? These questions were first answered in a seminal paper by Anderson [1958], where it was shown that for large enough strengths of disorder the diffusive motion of the electron will come to a halt. In particular, Anderson studied an unperturbed lattice of uncoupled sites, where the perturbation was considered to be the coupling between them, and randomness was introduced in the on-site energies. For this model he showed that for a large degree of randomness, the transmission of a wave decays exponentially with the length of the lattice.

This absence of wave diffusion in disordered mediums is nowadays called **Anderson localization**, and is a general wave phenomenon that applies to the transport of different types of classical or quantum waves, like electromagnetic, acoustic and spin waves. Its origin is the wave interference between multiple scattering paths; i.e. the introduction of randomness can drastically disturb the constructive interference, leading to the halting of waves. Anderson localization plays an important role in several physical phenomena. For example, the localization of electrons has dramatic consequences for the conductivity of materials, since the medium no longer behaves like a metal, but becomes an insulator when the strength of disorder exceeds a certain threshold. This transition is often referred to as the metal-insulator transition (MIT).

Often theoretical and numerical approaches of localization start with the Anderson model: a standard tight-binding (i.e. nearest-neighbor hopping) with an on-site potential disorder. This can be represented in one dimension by a time-dependent Schrödinger equation

$$i\frac{\partial \psi_l}{\partial t} = \epsilon_l \psi_l - \psi_{l+1} - \psi_{l-1}. \tag{1}$$

Here $\{\epsilon_l\}$ are the random on-site energies, which are drawn from an uncorrelated uniform distribution in $[-W/2, W/2]$, where W parametrizes the disorder strength. ψ_l is the complex wavefunction associated with lattice site l. Using the substitution, $\psi_l = A_l \exp(-i\lambda t)$ yields a time-independent form

$$\lambda A_l = \epsilon_l A_l - A_{l+1} - A_{l-1}. \tag{2}$$

The solution consists of both a set of eigenvectors called the **normal modes** (NMs), A_l^ν, (normalized as $\sum_l (A_l^\nu)^2 = 1$), and also a set of eigenvalues called the normal frequencies, $\lambda_\nu \in [-W/2 - 2, W/2 + 2]$ which exist in a spectral band of width $\Delta = 4 + W$. The eigenvectors are exponentially localized, meaning that their *asymptotic behavior* can be described by an exponential decay

$$|A_l^\nu| \sim e^{-l/\xi(\lambda_\nu)}, \tag{3}$$

where $\xi(\lambda_\nu)$ is a characteristic energy-dependent length, called the *localization length*. Naturally, $\xi \to \infty$ corresponds to an extended eigenstate. Several approaches have been developed for the evaluation of ξ, such as: the transfer matrix method, schemes based on the transport properties of the lattice, and perturbative techniques. For more information on such approaches, the reader is referred to [Kramer & MacKinnon, 1993] and references therein. In general, these approaches approximate the localization length as $\xi(\lambda_\nu) \approx 96/W^2$ for weak disorder strengths, $W \leq 4$. On average, the localization volume (i.e. spatial extent) V of the NM is on order of $3.3\xi(0)$ for these weak disorder strengths, and tends to unity in the limit of strong disorder.

In real experiments, measurements of transmission and conductivity are mainly performed, so the need for a connection between the conductivity and the spectrum becomes apparent. The basic approach towards the fulfillment of this goal was the establishment of a connection between the conductivity and the sensitivity to changes of the boundary conditions of the eigenvalues of the Hamiltonian of a finite (but very large) system [Edwards & Thouless, 1972]. The sensitivity to the boundary conditions turned out to be conceptually important for the formulation of a scaling theory for localization [Abrahams, 1979]. The main hypothesis of this single-parameter scaling theory is that close to the transition between localized and extended states, there should be only one scaling variable which should depend on the conductivity for the metallic behavior, and the localization length for the insulating behavior. This single parameter turned out to be a dimensionless conductance (often called *Thouless conductance* or *Thouless number*) defined as

$$g(N) = \frac{\delta E}{\Delta E}, \tag{4}$$

where δE is the average energy shift of eigenvalues of a finite system of size N due to the change in the boundary conditions, and ΔE is the average spacing of the eigenvalues. For localized states and large N, δE becomes very small and $g(N)$ exponentially vanishes. In the metallic regime the boundary conditions always influence the energy levels, even in the limiting case of infinite systems. The introduction of the Thouless conductance led to the formulation of a simple criterion for the occurrence of Anderson localization: $g(N) < 1$. In one- and two-dimensional random media this criterion can be reached for any degree of disorder by just increasing the size of the medium, while in higher dimensions a critical threshold exists.

The experimental observation of Anderson localization is not easy, for example, due to the electron-electron interactions in cases of electron localization, and the difficult discrimination between localization and absorption in experiments of photon localization. Nevertheless, nowadays the observation of Anderson localization has been reported in several experiments, a few of which we quote here. In [Wiersma *et al.*, 1997; Störzer *et al.*, 2006] localization of light in three-dimensional random media was reported. Anderson localization has also been observed in experiments of transverse localization of light for two- [Schwartz

et al., 2007] and one- [Lahini *et al.*, 2008] dimensional photonic lattices. Anderson localization has also been observed in experiments of localization of a Bose–Einstein condensate in an one-dimensional optical potential [Billy *et al.*, 2008; Roati *et al.*, 2008], and of elastic waves in a three-dimensional disordered medium [Hu *et al.*, 2008]. In addition, the observation of the MIT in a three-dimensional model with atomic matter waves has been reported [Chabé *et al.*, 2008].

1.2. *Wannier–Stark ladder–Bloch oscillations*

Another intriguing class of problems appears when replacing the disorder potential ϵ_l by a DC field $\epsilon_l = lE$ (E denotes the strength of the field). As an example, one can mention the textbook solid state problem of an electron in a periodic potential with an additional electric field (see e.g. [Tsu, 1993]) which leads to investigations of Bloch oscillations [Wannier, 1960] and Landau–Zener tunneling [Landau, 1932; Zener, 1932; Liu *et al.*, 2002] in different physical systems. Nowadays, such effects are experimentally observed by employing optical waves in photonic lattices [Pertsch *et al.*, 1999; Morandotti *et al.*, 1999] and ultracold atoms in optical lattices [Anderson & Kasevich, 1988; Gustavsson *et al.*, 2008; Morsch *et al.*, 2001]. If the well depth of the periodic potential is large enough, Landau–Zener tunneling is suppressed, the problem is discretized (Wannier–Stark ladder) and the resulting eigenvalue problem is explicitly solved in terms of the localized eigenmodes of the system (see e.g. [Fukuyama *et al.*, 1973]). Let us consider a discrete linear Schrödinger equation, as in Eq. (1) but now with a DC bias E:

$$i\dot{\psi}_l = lE\psi_l - \psi_{l+1} - \psi_{l-1}. \tag{5}$$

Note this is the governing equation e.g. for dilute Bose–Einstein condensate (BEC) dynamics in a deep and biased optical potential, whereby $|\psi_l(t)|^2$ implies BEC density in the lth potential well. Here, ψ_l is also a site's complex amplitude, and the same substitution as in Eqs. (1) and (2) can be made to arrive at the eigenvalue problem

$$\lambda A_l = lEA_l - A_{l+1} - A_{l-1}. \tag{6}$$

In the case of an infinite lattice, this yields eigenvalues of $\lambda_\nu = E\nu$ (with integer ν). These eigenvalues form an equidistant spectrum which extends over the whole real axis — the Wannier–Stark ladder.

The corresponding normal modes obey the generalized translational invariance $A_{l+\mu}^{\nu+\mu} = A_l^{\nu}$ [Wannier, 1960] and are given by the Bessel functions of the first kind, $A_l^{(0)} = J_l(2/E)$. All normal modes are spatially localized with an asymptotic decay of

$$|A_{l\to\infty}^{(0)}| \to \frac{\left(\frac{1}{E}\right)^l}{l!}.$$

The eigenstates are thus more strongly localized as compared to the disordered case, where the eigenstates decay exponentially. Remarkably, various observables exhibit temporal periodic motion (Bloch oscillations) with the period $T_B = 2\pi/E$.

The localization volume of an eigenstate is determined via $\mathcal{L} = 1/\sum_l |A_l^{(0)}|^4$. It characterizes the spatial extent of the eigenstate as a function of E. In Fig. 1, the localization volume of an eigenstate is shown as a function of E. The asymptotic behavior was found to be $\mathcal{L} \propto -[E \cdot \ln E]^{-1}$ for $E \to 0$, and $\mathcal{L} \to 1$ for $E \to \infty$ [Krimer et al., 2009].

1.3. *Aubry–André chains — An example of quasiperiodicity*

A periodic lattice gives a translational symmetry. A simple way to destroy the symmetry is to introduce a secondary periodic lattice of a different and
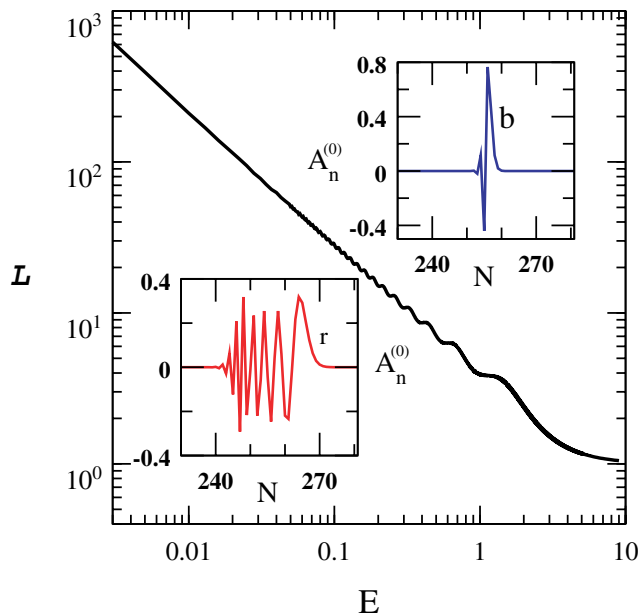

Fig. 1.   Localization volume $\mathcal{L}$ of the eigenfunction $A_n^{(0)}$ versus E. Insets: Explicit form of the eigenfunction across the chain for two values $E = 2$ and $E = 0.2$ [(b), blue; (r), red]. Figure adapted from [Krimer et al., 2009].

incommensurate frequency. This idea has gained much attention in solid-state via *quasicrystals* [Levine & Steinhardt, 1984; Trebin, 2003; Vekilov & Chernikov, 2010]. The idea of incommensuration also extends into optics via sequenced (e.g. Fibonacci, Thue–Morse, Rudin–Shapiro) potentials [Maciá & Domínguez-Adame, 2000; Albuquerque & Cottam, 2003]. More so, it has recently been focused on ultracold atomic physics, in terms of *bichromatic* lattices [Guidoni et al., 1997; Modugno, 2009, 2010; Albert & Leboeuf, 2010].

Regardless of the subfield, for large lattices the dynamics is described in a tight-binding form — as in Eqs. (1) and (5) — and goes by the moniker of *Aubry–André model*

$$i\frac{\partial\psi_l}{\partial t} = \zeta \cos(2\pi\alpha l) \cdot \psi_l - \psi_{l+1} - \psi_{l-1} \qquad (7)$$

in which the parameter α dictates the commensurability ratio between the two different frequencies. The parameter ζ dictates a relative lattice strength, much as W for the disordered Anderson model. As in Eqs. (2) and (6), a substitution is made to turn Eq. (7) into an eigenvalue problem:

$$\lambda A_l = \zeta \cos(2\pi\alpha l) \cdot A_l - A_{l+1} - A_{l-1}. \qquad (8)$$

Originally this model was introduced by Harper [1955b, 1955a] [hence Eq. (7) is also synonymously the *Harper model*] to describe a low-temperature two-dimensional electron gas in a high magnetic field, in which the parameter α describes incommensurability between the quantum of magnetic flux and the lattice cell. It is commonplace to make the lattice as largely incommensurate as possible for studies in the Aubry–André model; the inverse golden mean is often used $\alpha = (\sqrt{5} - 1)/2$. We shall henceforth keep with this standard convention.

Using the Fourier form $\psi_l = \sum_k e^{2\pi i \alpha k l} \phi_k$, Eq. (7) transforms into the quasi-momentum basis of $\{\phi_k\}$

$$i\frac{\partial\phi_k}{\partial t} = 2\cos(2\pi\alpha k) \cdot \phi_k - \frac{\zeta}{2}\phi_{k+1} - \frac{\zeta}{2}\phi_{k-1}. \qquad (9)$$

Note that Eqs. (7) and (9) are **not** identical, as seen in the location of ζ parameter. Equation (7) dictates dynamics in a position representation and ζ occurs on the on-site energy terms, while Eq. (9) dictates dynamics in a momentum representation, and ζ appears in the kinetic coupling of the momentum modes. Even though the two equations are strictly different, under exchange of ζ the two

equations are equivalent in form — a property known as *self-duality*, first derived by Aubry and André [1980]. Both equations can easily be seen to be equivalent without ANY parameter exchange if $\zeta = 2$. This self-dual symmetry is nicely observed in the eigenstates. For the critical value of $\zeta = 2$, the two representations have identical localization lengths. Additionally, the localization volumes can be probed as in the prior section, using either $\mathcal{L}_\psi = 1/\sum_l |\psi_l|^4$ or $\mathcal{L}_\phi = 1/\sum_k |\phi_k|^4$. This is shown in Fig. 2. In the figure, for small ζ, states localized in position space are extended in momentum space. As ζ sweeps across $\zeta = 2$, the strong transition from localized to extended is seen for $\mathcal{L}_\psi$ (and vice-versa for $\mathcal{L}_\phi$).

The value $\zeta = 2$ is thus tied strongly to criticality and fractality of eigenstates, whose existence in quasiperiodic models has been quite an active hotbed. In terms of the Aubry–André model, this has focused on changes in the density of states [Soukoulis & Economou, 1982], density–density correlations [Boers *et al.*, 2007; Li *et al.*, 2010], Husimi/Wigner distributions [Ingold *et al.*, 2002; Aulbach *et al.*, 2004], and spreading of density moments [Hu *et al.*, 2000; Hufnagel *et al.*, 2001; Diener *et al.*, 2001]. The Aubry–André model has also seen modification by another parameter ν,
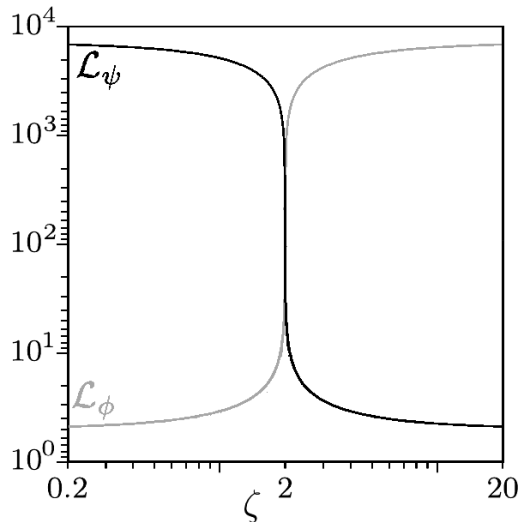

Fig. 2. The self-duality of the Aubry–André model: For lattice size of 10 946, as a function of the parameter ζ is shown the average localization volumes in both real space ($\mathcal{L}_\psi$, black) and momentum space ($\mathcal{L}_\phi$, gray). For small $\zeta < 2$, the eigenstates are extended in real space ($\mathcal{L}_\psi \gg 1$) and localized in momentum space ($\mathcal{L}_\psi \sim 1$). At $\zeta = 2$ the exchange is seen, i.e. for $\zeta > 2$ we see the eigenstates localized in real space and extended in momentum space. Figure adapted from those shown in [Aulbach *et al.*, 2004].

introduced in Eq. (7) as $\cos(2\pi\alpha l) \mapsto \cos(2\pi\alpha n^\nu)$, in order to further probe and control the mobility edge [Griniasty & Fishman, 1988; Sarma *et al.*, 1988; Varga *et al.*, 1992]. Study of the Aubry–André model continues onward, beyond simple tight-binding formalisms [Johansson & Riklund, 1991; Biddle *et al.*, 2009].

1.4. *Quantum kicked rotor — Localization in momentum space*

There is a growing interest in the study of quantum systems with time-dependent Hamiltonians. An important motivation in this area is a better understanding of the quantum dynamics within simple systems whose classical counterparts exhibit chaotic behavior. One of the relatively simple models to study quantum dynamics is a quantum kicked rotor. This model was introduced in [Casati *et al.*, 1979] as a quantum analog of *the standard mapping* [Chirikov, 1979], which is the basic model of dynamical chaos in the classical limit. In spite of this formal analogy, the dynamical chaos in the quantum kicked rotor exhibits some specific features closely related with the quantum nature of the underlying model. Namely, in the classical case the motion depends on a single parameter, K, the dimensionless strength of kick. For each value of K the motion can be quasi-periodic, chaotic, or accelerating, depending on the initial conditions. At small K the chaotic regions are isolated and separated by the Kolmogorov–Arnold–Moser (KAM) trajectories; consequently the motion is bounded. For $K = K_c \approx 0.97146$, the last of these trajectories disappears and diffusion in the momentum space takes place. On the other hand, in the quantum case the energy remains bounded and does not increase with time even for $K > K_c$. In other words, the quantum suppression of classical diffusion in the phase space has taken place in the model of quantum kicked rotor [Izrailev, 1990]. The quantum localization of classical chaotic diffusion is sometimes called *dynamical localization*. This phenomenon is in many aspects analogous to Anderson localization in the models with disorder [Fishman *et al.*, 1982]. However, in the case of quantum chaos there is no randomness and transient diffusion in the corresponding classical system. In other words, the dynamical localization in a quantum kicked rotor occurs in a completely deterministic system. In addition, in the cases where the period of kicks

equals to an integer multiple of the natural period of rotor, quantum resonances and ballistic diffusion occur.

The quantum kicked rotor is described by the Schrödinger equation:

$$i\frac{\partial\psi}{\partial t} = \hat{H}\psi$$
$$= -\frac{1}{2}\frac{\partial^2\psi}{\partial\theta^2} + k\cos(\theta)\psi \sum_{m=-\infty}^{+\infty} \delta(t - mT).$$
(10)

Here, θ and $-i\partial/\partial\theta$ are the position and the conjugated momentum operators of the rotor. All quantities are in units of $\hbar = 1$, and the motion is considered on a ring with periodic boundary conditions $\psi(\theta + 2\pi) = \psi(\theta)$. The parameter k is the kick strength and T is the period between kicks. The evolution operator over one period T is given by

$$\hat{U} = \exp\left(-i\frac{T}{2}\frac{\partial^2}{\partial\theta^2}\right)\exp(-ik\cos(\theta)).$$
(11)

The solution $\psi(\theta, t)$ of Eq. (10) can be expanded on the basis of the angular momentum eigenfunctions in a form

$$\psi(\theta, t) = \frac{1}{\sqrt{2\pi}}\sum_{n=-\infty}^{\infty} A_n(t)\exp(in\theta),$$
(12)

where the coefficients $A_n(t)$ are the Fourier coefficients of the time-dependent wave function $\psi(\theta, t)$. As a result of the action of the evolution operator, Eq. (11), on the wave function $\psi(\theta, t)$ over one period T, the following mapping of the Fourier coefficients A_n is obtained

$$A_n(t + T)$$
$$= \sum_m (-i)^{n-m} J_{n-m}(k) A_m(t) \exp\left(-i\frac{1}{2}Tm^2\right),$$
(13)

where $J_{n-m}(k)$ is the Bessel function of the first order [Casati et al., 1979]. It is found from Eq. (13) that — opposite to the classical model where one parameter determines the system behavior — in the quantum model, behavior depends on two parameters: k and T [Izrailev, 1990]. The perturbation strength k gives the effective number of unperturbed states covered by one kick, and T is the ratio between the period of kicks T and the

natural period of rotor, set to one in this case. When the ratio between these two periods is rational (i.e. T is a rational number), the rotor energy $E(t) = \sum_n |A_n(t)|^2 n^2/2$, grows ballistically in time as t^2, at variance to the classical case. This phenomenon is called quantum resonance (being caused by pure quantum interference effects) and has no relation to the classical behavior [Casati et al., 1979]. On the other hand, for irrational T, suppression of the energy diffusion occurs and the spreading of the wave packet stops. Equation (13) can be also treated as an eigenvalue problem

$$\lambda_\nu A_n^\nu = \sum_m (-i)^{n-m} J_{n-m}(k) \exp\left(-i\frac{1}{2}Tm^2\right) A_m^\nu.$$
(14)

The complex eigenvectors are localized for irrational T; $|A_{n\to\infty}^\nu| \to 0$. The characteristic eigenvalues λ_ν are complex numbers placed on the unit circle in the complex plane, $\lambda_\nu = \exp(i\chi_\nu)$. For rational T then, extended eigenvectors are obtained.

One of the first experimentally-grounded evidences of localization in a quantum system (which leads to the suppression of the chaotic diffusion in the action space) was obtained with hydrogen atoms in a microwave field [Bayfield et al., 1989]. The quantum energy spectrum of this system — which consists of excited hydrogen atoms inside an intense time dependent magnetic field — is investigated in the regime when underlying classical motion has passed from regular to irregular behavior, via increasing magnetic field strength [Delande & Gay, 1987]. The first experimental realization of the quantum kicked rotor was obtained in a sample of dilute ultracold sodium atoms in a periodic standing wave of near-resonant light, pulsed periodically in time to approximate a series of delta kicks [Moore et al., 1995]. In these experiments, atomic momenta were measured as a function of interaction time and the pulse period. The diffusive growth of energy up to a quantum break time, followed by dynamical localization, was observed. In addition, in cases with the pulse period equal to an integer multiple of the rotor period, the ballistic diffusion and corresponding quantum resonances were observed. All these experimental findings confirmed previously established numerical and theoretical predictions of the quantum kicked rotor model.

2. Nonlinear Waves: Destruction of Localization

2.1. *Disorder*

A number of recent studies have been devoted to uncover the interplay of nonlinearity and disorder [Molina, 1998; Pikovsky & Shepelyansky, 2008; Kopidakis *et al.*, 2008; Flach *et al.*, 2009; Skokos *et al.*, 2009; Veksler *et al.*, 2009; Mulansky *et al.*, 2009; Skokos & Flach, 2010; Flach, 2010; Laptyeva *et al.*, 2010; Basko, 2011]. Most of these studies consider the evolution of an initially localized wave packet. While the linear equations will trap the packet, the presence of nonlinearity leads to a spreading of the packet well beyond the limits set by the linear theory. Numerical studies suggest that the second moment m_2 of the wave packet grows subdiffusively in time following a power law t^α with $\alpha < 1$. On the other hand, for weak enough nonlinearity, wave packets appear to be frozen over the complete available integration time, thereby resembling Anderson localization, at least on finite time scales. As recently argued by Johansson *et al.* [2010], these states may be localized for infinite times and correspond to Kolmogorov–Arnold–Moser (KAM) torus structures in phase space.

2.1.1. *Basic models*

Let us consider as our first model the disordered nonlinear Schrödinger (DNLS) chain, which has equations of motion

$$i\frac{\partial \psi_l}{\partial t} = \epsilon_l \psi_l - \psi_{l+1} - \psi_{l-1} + \beta |\psi_l|^2 \psi_l \quad (15)$$

with a nonlinearity strength β and random on-site energies chosen as in Eq. (1).

A second model we consider is the Klein–Gordon (KG) chain of coupled anharmonic oscillators

$$\frac{\partial^2 u_l}{\partial t^2} = -\tilde{\epsilon}_l u_l - u_l^3 + \frac{1}{W}(u_{l+1} + u_{l-1} - 2u_l), \quad (16)$$

where $\tilde{\epsilon}_l$ are uncorrelated random values chosen uniformly in the interval $[1/2, 3/2]$. Note in this model, u_l is the generalized coordinate on the site l and is wholly real, as opposed to Eq. (15)'s complex ψ_l values. Nevertheless, we can reduce the linear form of Eq. (16) [remove the cubic u_l^3 term] to the same eigenvalue form as Eq. (2). This is done with the transforms $\epsilon_l = W(\tilde{\epsilon}_l - 1)$ and $\lambda_\nu = W\omega_\nu^2 - W - 2$, where ω_ν are the KG's eigenfrequencies, $\omega_\nu^2 \in [1/2, 3/2 + 4/W]$. The width

of the KG's **squared** eigenfrequency spectrum is then $\Delta = 1 + 4/W$.

Additionally, in the KG model the total energy

$$E = \sum_l \mathcal{E}_l$$

where

$$\mathcal{E}_l \equiv \frac{1}{2}\left(\frac{\partial u_l}{\partial t}\right)^2 + \frac{1}{2}\tilde{\epsilon}_l u_l^2 + \frac{1}{4}u_l^4 + \frac{1}{2W}(u_{l+1} - u_l)^2$$

$$\geq 0$$

acts as the nonlinear control parameter, similar to β for the DNLS case. Both models conserve the total energy; additionally, the DNLS conserves the total norm $\mathcal{S} = \sum_l |\psi_l|^2$. For small amplitudes, an approximate mapping, $\beta\mathcal{S} \approx 3WE$, from the KG model to the DNLS model exists [Kivshar & Peyrard, 1992; Kivshar, 1993; Johansson, 2006]. Because of this mapping, in the remainder of this section we shall focus on the DNLS model's analytics, and return to the KG model only in our observations.

The average spacing d of eigenvalues of NMs within the range of a localization volume is of the order of $d \approx \Delta/V$, which becomes $d \approx \Delta W^2/300$ for weak disorder. The two frequency scales $d < \Delta$ are expected to determine the packet evolution details in the presence of nonlinearity.

The equations of motion in Eq. (15) can be rewritten in normal mode space as

$$i\dot{\phi}_\nu = \lambda_\nu \phi_\nu + \beta \sum_{\nu_1, \nu_2, \nu_3} I_{\nu,\nu_1,\nu_2,\nu_3} \phi_{\nu_1}^* \phi_{\nu_2} \phi_{\nu_3} \quad (17)$$

where the variables $\phi_\nu = \sum_l A_l^\nu \psi_l$ determine the complex time-dependent behavior of the NMs and $I_{\nu,\nu_1,\nu_2,\nu_3} = \sum_l A_{\nu,l} A_{\nu_1,l} A_{\nu_2,l} A_{\nu_3,l}$ are the overlap integrals. The frequency shift of a single site oscillator induced by the nonlinearity is $\delta \sim \beta n$ for DNLS (here $n = |\psi|^2$), and $\delta \sim \mathcal{E}$ for the KG model [Skokos *et al.*, 2009; Laptyeva *et al.*, 2010].

We sort the NMs with increasing center-of-norm coordinate $X_\nu = \sum_l l(A_l^\nu)^2$. For DNLS, we monitor the time-dependent normalized norm density distribution in NM space, $z_\nu \equiv n_\nu/\sum_\mu n_\mu$. The KG counterpart is the normalized energy density distribution in NM space $z_\nu \equiv \mathcal{E}_\nu/\sum_\mu \mathcal{E}_\mu$. We characterize distributions by means of the second moment $m_2 = \sum_\nu (\nu - \bar{\nu})^2 z_\nu$ (where $\bar{\nu} = \sum_\nu z_\nu$), which quantifies the wave packet's degree of spreading, and the participation number $P = 1/\sum_\nu z_\nu^2$, which measures the number of effectively excited

sites. The ratio $\zeta = P^2/m_2$ (the compactness index [Skokos *et al.*, 2009]) quantifies the sparseness of a packet.

2.1.2.   *Regimes of wave packet spreading*

We consider compact wave packets at $t = 0$ spanning a width L centered in the lattice, such that within L there is a constant norm density of n and a random phase at each site (outside the volume L the norm density is zero). In the KG case, this corresponds to exciting each site in the width L with the same energy density, $\mathcal{E} = E/L$, i.e. setting initial momenta to $p_l = \pm\sqrt{2\mathcal{E}}$ with randomly assigned signs. If $\delta \geq \Delta$ then a substantial part of the wave packet will be self-trapped [Kopidakis *et al.*, 2008; Skokos *et al.*, 2009]. This is due to nonlinear frequency shifts, which will tune the excited sites immediately out of resonance with the nonexcited neighborhood [Flach & Willis, 1998; Flach & Gorbach, 2008]. In fact, partial self-trapping will occur already for $\delta \geq 2$ since at least some sites in the packet may be tuned out of resonance. If now $\delta < 2$, self-trapping is avoided, and the wave packet can start to spread. For $L < V$, the packet will spread over the localization volume during the time $\tau_{\mathrm{lin}} \approx 2\pi/d$ (even for $\beta = 0$). At that time, the new norm density will drop down to $n(\tau_{\mathrm{lin}}) \approx (nL)/V$. For $L > V$ the norm density will not change appreciably up to τ_{lin} and $n(\tau_{\mathrm{lin}}) \approx n$. The nonlinear frequency shift $\beta n(\tau_{\mathrm{lin}})$ should be now compared with the average spacing d. If $\beta n(\tau_{\mathrm{lin}}) > d$, all NMs in the packet are resonantly interacting with each other. We refer to this regime as strong chaos. If instead $\beta n(\tau_{\mathrm{lin}}) < d$, NMs are weakly interacting with each other. We refer to this regime as weak chaos. Note that a spreading wave packet that is launched in the regime of strong chaos will increase in size, drop its norm (energy) density, and therefore the crossover into the asymptotic regime of weak chaos must occur at later times. For a single-site excitation $L = 1$ the strong chaos regime shrinks to zero width in the norm/energy parameter and one is left only with either weak chaos or self-trapping [Pikovsky & Shepelyansky, 2008; Flach *et al.*, 2009; Skokos *et al.*, 2009; Veksler *et al.*, 2009]. To summarize, the expected spreading regimes for $L \geq V$ are:

$$\delta > 2 : \text{onset of self-trapping};$$
$$d < \delta < 2 : \text{strong chaos}; \qquad (18)$$
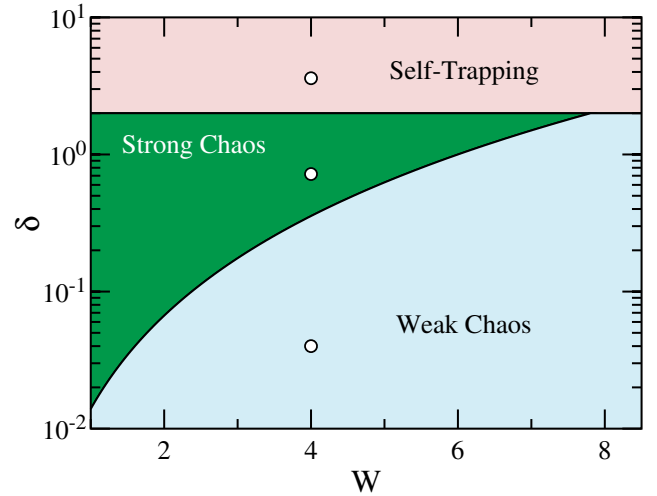$$\delta < d : \text{weak chaos}.$$

Fig. 3.   Parametric space of disorder, W, versus the frequency shift induced by nonlinearity, δ, for the DNLS model. The KG analog is obtained by the small amplitude mapping. Three spreading regimes are shown for dynamics dictated by: (i) weak chaos (pale blue), (ii) strong chaos (green), and (iii) the onset of self-trapping (pale red). The three circles show numerical values used in Fig. 4. Adapted from [Laptyeva *et al.*, 2010].

Figure 3 sketches the predicted regimes in a parametric space for the case $L = V$, in which lines represent the regime boundaries $\delta = d$ and $\delta = 2$. Note that we used $d = \Delta/(3.3\xi(0))$ with $\xi(0) = 96W^{-2}$ being the weak disorder estimate.

2.1.3.   *Resonances and chaos*

A NM with index μ in a layer of width V in the cold exterior — which borders the packet but will belong to the core of the spreading packet at later time — is either incoherently *heated* by the packet, or *resonantly* excited by some particular NM from a layer with width V inside the packet. The resonant channel will lead to spreading only if a new resonance can be found. Due to the disorder this is not possible. Then a single resonance will simply lead to beatings (oscillations) of the wave packet. In order to finally achieve true spreading, we have to destroy the phase coherence of the wave packet. Therefore there is no other way but to allow incoherent chaotic dynamics to take place, if spreading is observed.

Chaos is a combined result of resonances and nonintegrability. Let us estimate the number of resonant modes in the packet for the DNLS model. Excluding secular interactions, the amplitude of a NM with $|\phi_\nu|^2 = n_\nu$ is modified by a triplet of other

modes $\boldsymbol{\mu} \equiv (\mu_1, \mu_2, \mu_3)$ in first order in β as

$$|\phi_\nu^{(1)}| = \beta\sqrt{n_{\mu_1} n_{\mu_2} n_{\mu_3}} \cdot R_{\nu,\boldsymbol{\mu}}^{-1},$$

$$R_{\nu,\boldsymbol{\mu}} \sim \left| \frac{\mathbf{d\lambda}}{I_{\nu,\mu_1,\mu_2,\mu_3}} \right|, \qquad (19)$$

where $\mathbf{d\lambda} = \lambda_\nu + \lambda_{\mu_1} - \lambda_{\mu_2} - \lambda_{\mu_3}$. The perturbation approach breaks down, and resonances set in, when $\sqrt{n_\nu} < |\phi_\nu^{(1)}|$. Since all considered NMs belong to the packet, we assume their norms to be equal to n. The main result is that the probability of a packet mode to be resonant is given by $\mathcal{P} = 1 - e^{-C\beta n}$ [Krimer & Flach, 2010], with C being a constant depending on the strength of disorder. Then

$$m_2 \sim \mathcal{D}\, t, \quad \mathcal{D} \sim \beta^2 n^2 [\mathcal{P}(\beta n)]^2 \qquad (20)$$

and finally

$$n^{-2} \sim \beta[1 - e^{-C\beta n}]t^{1/2}. \qquad (21)$$

The solution of this equation yields a crossover from subdiffusive spreading in the regime of strong chaos to subdiffusive spreading in the regime of weak chaos:

$$m_2 \sim \begin{cases} [\beta^2 t]^{1/2}, & C\beta n > 1 \text{ (strong chaos)}; \\ [\beta^4 t]^{1/3}, & C\beta n < 1 \text{ (weak chaos)}. \end{cases} \qquad (22)$$

The only characteristic frequency scale here is $1/C$. From the above discussion of the different spreading regimes it follows that $1/C \approx d$.

2.1.4. *Computational results*

Ensemble averages over disorder were calculated for 1000 realizations with $W = 4$ and are shown in Fig. 4 (upper row). We use $L = V = 21$ and system sizes of 1000–2000 sites. For DNLS, an initial norm density of $n = 1$ is taken, so that $\delta = \beta$. The values
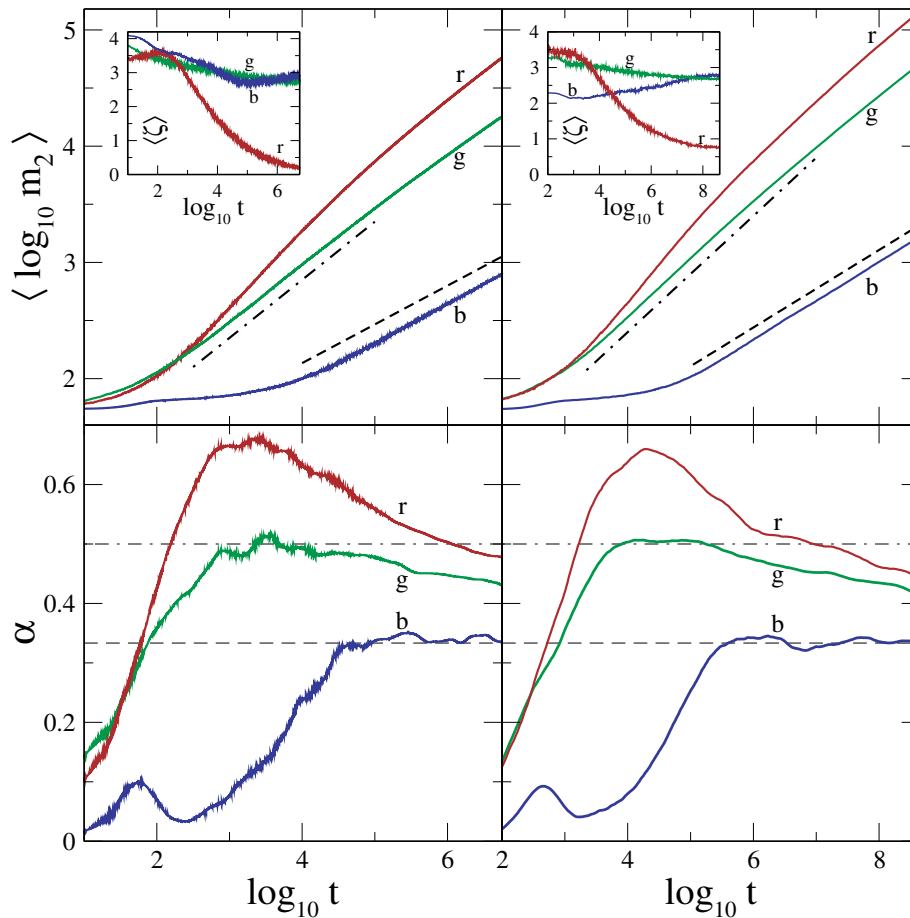

Fig. 4. Upper row: Average log of second moments (inset: average compactness index) versus log time for the DNLS/KG on the left/right, for $W = 4, L = 21$. Colors/letters correspond to three different regimes: (i) weak chaos — (b)lue, $\beta = 0.04$ ($\mathcal{E} = 0.01$), (ii) strong chaos — (g)reen, $\beta = 0.72$ ($\mathcal{E} = 0.2$), (iii) self-trapping — (r)ed, $\beta = 3.6$ ($\mathcal{E} = 0.75$). The respective lighter surrounding areas show one standard deviation error. Dashed lines are to guide the eye to $\sim t^{1/3}$, while dot-dashed guides for $\sim t^{1/2}$. Lower row: Finite difference derivatives $\alpha(\log t) = d\langle \log m_2 \rangle/d \log t$ for the smoothed m_2 data respectively from the above curves. Adapted from [Laptyeva *et al.*, 2010].

of β ($\mathcal{E}$ for KG) are chosen to give three expected spreading regimes (see Fig. 3), respectively $\beta \in \{0.04, 0.72, 3.6\}$ and $\mathcal{E} \in \{0.01, 0.2, 0.75\}$. In the predicted regime of weak chaos, we indeed find a subdiffusive growth of m_2 according to $m_2 \sim t^\alpha$ with $\alpha \approx 1/3$ at large times. In the expected regime of strong chaos, we observe exponents $\alpha \approx 1/2$ for $10^3 \lesssim t \lesssim 10^4$ (KG: $10^4 \lesssim t \lesssim 10^5$) in Fig. 4. Time averages in these regions over the green curves yield $\alpha \approx 0.49 \pm 0.01$ (KG: 0.51 ± 0.02). With spreading continuing in the strong chaos regime, the norm density in the packet decreases, and eventually satisfies $\beta n \leq d$. That leads to a dynamical crossover to the slower weak chaos subdiffusive spreading, as predicted. Fits of the further decay suggest $\alpha \approx 1/3$ at $10^{10} \lesssim t \lesssim 10^{11}$. In the regimes of weak and strong chaos, the compactness index at largest computational times is $\zeta \approx 2.85 \pm 0.79$ (KG: 2.74 ± 0.83), as seen in the blue and green curves of Fig. 4. This means that the wave packet spreads, but remains rather compact and thermalized ($\zeta \approx 3$). The duration of $\alpha = 1/2$ spreading (and the crossover time) is largely dependent on how deep we are initially in the strong chaos regime. This is illustrated in Fig. 5 for the KG model. For $W \in \{1, 2\}$ a long-lasting strong chaos spreading is clearly observed. For $W \in \{4, 6\}$ the width in the energy density is small and, even if,
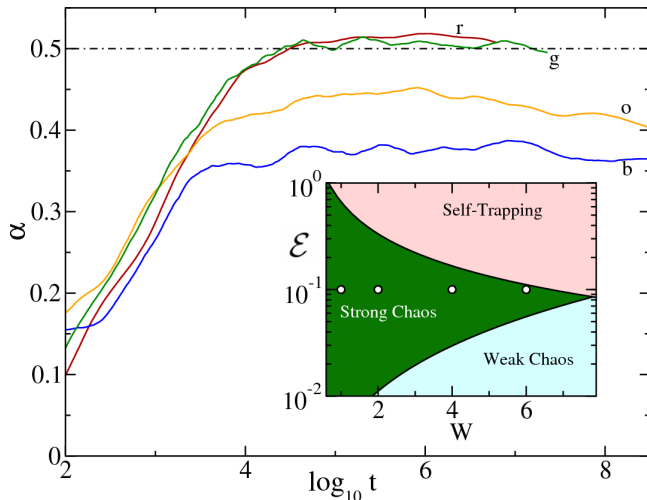

Fig. 5. Spreading behavior in the strong chaos regime for the KG model, with an initial energy density of $\mathcal{E} = 0.1$. The four curves are for the disorder strengths of: $W = 1$ — (r)ed, $W = 2$ — (g)reen, $W = 4$ — (o)range, $W = 6$ — (b)lue. Inset: the KG analog of the DNLS parametric space from Fig. 3. The four points correspond to the disorder strengths used in the main portion of the figure. Adapted from [Laptyeva *et al.*, 2010].

initially, the energy density is chosen to give strong chaos, its decrease due to spreading will get the system into the weak chaos regime with $\alpha < 1/2$.

2.1.5. *Generalizations*

Let us apply the same theoretical arguments to a general **D**-dimensional lattice with the nonlinearity of the order σ:

$$i\dot{\psi}_\mathbf{l} = \epsilon_\mathbf{l} \psi_\mathbf{l} - \beta|\psi_\mathbf{l}|^\sigma \psi_\mathbf{l} - \sum_{\mathbf{m} \in \mathbf{D(l)}} \psi_\mathbf{m}. \qquad (23)$$

Here $\mathbf{l}$ denotes a **D**-dimensional lattice vector with integer components, and $\mathbf{m} \in \mathbf{D(l)}$ defines its set of nearest neighbors. We assume that all NMs are spatially localized (which can be obtained for strong enough disorder W). A wave packet with the same average norm n per excited mode has a second moment $m_2 \sim n^{-2/\mathbf{D}}$. The nonlinear frequency shift is proportional to $\beta n^{\sigma/2}$.

A straightforward generalization of the expected regimes of wave packet spreading [Flach, 2010] with $L \geq V$ leads to the following: self-trapping if $\beta n^{\sigma/2} > \Delta$, strong chaos if $\beta n^{\sigma/2} > d$, and weak chaos if $\beta n^{\sigma/2} < d$. The regime of strong chaos can be observed for $n > [d/\beta]^{2/\sigma}$.

Similar to the above we obtain a diffusion coefficient

$$\mathcal{D} \sim \beta^2 n^\sigma [\mathcal{P}(\beta n^{\sigma/2})]^2. \qquad (24)$$

In both regimes of strong and weak chaos the spreading is subdiffusive [Flach, 2010]:

$$m_2 \sim \begin{cases} [\beta^2 t]^{\frac{2}{2+\sigma\mathbf{D}}}, & \text{(strong chaos)}; \\ [\beta^4 t]^{\frac{1}{1+\sigma\mathbf{D}}}, & \text{(weak chaos)}. \end{cases} \qquad (25)$$

The number of resonances on the wave packet surface is $N_{RS} \sim \beta n^{\frac{\mathbf{D}(\sigma-2)+2}{2\mathbf{D}}}$. This number increases with time for

$$\mathbf{D} > \mathbf{D}_c = \frac{1}{1 - \dfrac{\sigma}{2}}, \quad \sigma < 2. \qquad (26)$$

We expect that the wave packet surface will not stay compact if Eq. (26) is fulfilled [Flach, 2010]. Instead, surface resonances will lead to a resonant leakage of excitations into the exterior. This process will increase the surface area, and therefore lead to even more surface resonances, which increase the surface area further on. The wave packet will fragmentize, perhaps get a fractal-like structure, and lower its compactness index. The spreading of the

wave packet will speed up, but will not anymore be due to pure incoherent transfer, instead it will become a complicated mixture of incoherent and coherent transfer processes. For such cases, Anderson localization will be destroyed quickly even in the tails of wave packets [Skokos & Flach, 2010].

The numerical evidence [Skokos & Flach, 2010] for the validity of predictions Eq. (25) for the generalized KG model $\ddot{u}_l = -\tilde{\epsilon}_l u_l - |u_l|^\sigma u_l + (1/W)(u_{l+1} + u_{l-1} - 2u_l)$ and energies away from the self-trapping regime are presented in Fig. 6. The energy values used there cross the boundary between the weak and strong chaos regimes around the interval $1 \lesssim \sigma \lesssim 2$. In particular, the computed exponents are in good agreement with the theoretical prediction for weak chaos [Eq. (25)] for $\sigma \geq 2$. For smaller values of σ they smoothly cross over to the prediction of strong chaos, as expected.

2.2. *Wannier–Stark ladder*

The evolution of a wave packet in a nonlinear Wannier–Stark ladder was studied in [Krimer *et al.*, 2009]. Nonlinearity induces frequency shifts and mode–mode interactions and destroys localization. For large strength of nonlinearity we observe single-site trapping as a transient, with subsequent explosive spreading, followed by subdiffusion. For moderate nonlinearities an immediate subdiffusion takes place. Finally, for small nonlinearities we find linear Wannier–Stark localization as a transient, with subsequent subdiffusion. For single-mode
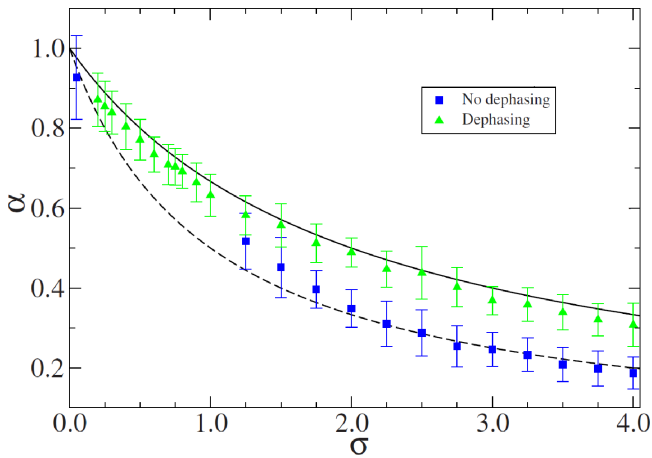

Fig. 6. Spreading exponent α versus the nonlinearity power σ for integration without dephasing (filled squares) and for integration with dephasing of NMs (filled triangles). The theoretically predicted boundaries of weak chaos and strong chaos are plotted by dashed and solid lines, respectively. Adapted from [Skokos & Flach, 2010].

excitations, additional stability and instability intervals with respect to the DC bias strength were shown to exist. The onset of subdiffusive spreading was also observed in [Datta & Jayannavar, 1998; Kolovsky *et al.*, 2010] for two runs on rather short scales up to $t = 10^5$.

2.2.1. *Basic model*

We consider the discrete nonlinear Schrödinger equation with a DC bias E

$$i\frac{\partial \psi_l}{\partial t} = lE\psi_l - \psi_{l+1} - \psi_{l-1} + \beta|\psi_l|^2\psi_l. \quad (27)$$

As in Eq. (17), a transformation to the NM space is first made using $\phi_\nu = \sum_l A_l^\nu \exp(-i\lambda_\nu t)$. The linear term can be gauged out by using a secular normal form $\phi_\nu = \chi_\nu \exp(-i\nu E t)$, yielding

$$i\frac{\partial \chi_\nu}{\partial t}$$
$$= \beta \sum_{\nu_1,\nu_2,\nu_3} I_{\nu,\nu_1,\nu_2,\nu_3} \chi_{\nu_1}^* \chi_{\nu_2} \chi_{\nu_3} e^{i(\nu+\nu_1-\nu_2-\nu_3)Et},$$
$$(28)$$

where

$$I_{\nu,\nu_1,\nu_2,\nu_3} \equiv \sum_n A_{n-\nu}^{(0)} A_{n-\nu_1}^{(0)} A_{n-\nu_2}^{(0)} A_{n-\nu_3}^{(0)} \quad (29)$$

are the overlap integrals between the NMs. As for DNLS with disorder, adding nonlinearity again leads to a finite range interaction between the eigenstates. The main difference from the disordered case is that here, the linear spectrum is unbounded and exact resonances are always present. Resonant normal form equations are indeed obtained by substituting $\nu + \nu_1 - \nu_2 - \nu_3 = 0$ into Eq. (28). These equations are not integrable [Krimer *et al.*, 2009], in contrast to the resonant normal form equations for the disordered case [Flach, 2010]. As a consequence, if at least two neighboring NMs are excited, the resonant normal form, having a connectivity similar to the original lattice equations, allows spreading over the whole lattice. Such a direct resonant interaction mechanism takes place between the NMs both inside and outside the wave packet.

2.2.2. *Single site excitation*

First, we study a single site initial excitation $\psi_l(0) = \delta_{l0}$. In that case the amplitudes in NM space are $\phi_\nu(0) = J_\nu(2/E)$. The nonlinear frequency shift, $\delta \sim \beta$, at site $n = 0$ should be compared with the
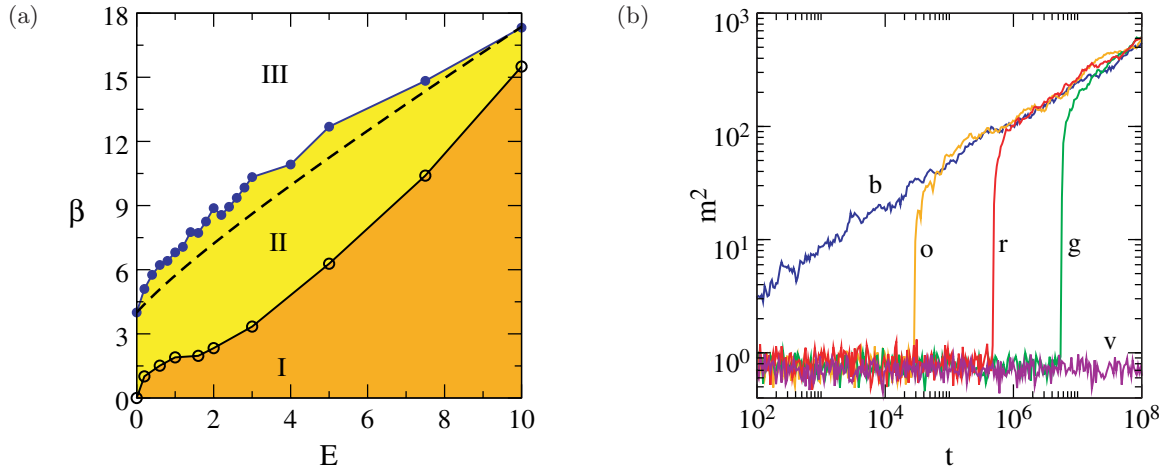
Fig. 7.   (a) The diagram of the three regimes of spreading in the parameter space (β, E) for Eq. (27). Empty and filled circles: numerically obtained thresholds which separate the three different regimes I, II, III — lines connecting symbols are meant to guide the eye for the boundaries. Black dashed line: threshold between II and III obtained from the dimer model. In the limit of $E \to \infty$, all lines merge to the asymptotic limit $\beta \propto E$. (b) Single site excitation for $E = 2$. Second moment m_2 versus time in log–log plots for different values of β inside the interval where an explosive delocalization of the trapped regime occurs: $\beta = 8.15, 8.25, 8.5$ [(o) orange; (g) green; (r) red]. $\beta = 8$ [(b), blue]: intermediate regime. $\beta = 8.9$ [(v), violet]: trapped regime. Figure adapted from [Krimer *et al.*, 2009].

two scales set by the linear problem: the eigenvalue spacing E and the eigenvalue variation over a localization volume $\Delta \equiv E\mathcal{L}$ (see Sec. 1.2). We found three qualitatively different regimes of spreading shown on the phase diagram in the parameter plane of nonlinearity, β, and DC field, E, strengths [see Fig. 7(a)]: (I) $\delta < E$, (II) $E < \delta < \Delta$, (III) $\Delta < \delta$. In case (I), the nonlinear frequency shift is less than the spacing between excited modes. Therefore no initial resonance overlap is expected, and the dynamics may evolve as that for $\beta = 0$ at least for long times. In case (II), resonance overlap happens, and the packet expands subdiffusively from the very beginning. For case (III), δ tunes the excited site out of resonance with the neighboring NMs. Resonances with more distant NMs are possible, but the overlap with these NMs is weaker the further away they are. Therefore for long times the excited site may evolve as an independent oscillator (trapping).

Let us discuss case (III) in more detail. For $E = 2$ and $\beta > 8.9$, the single site excitation stays trapped up to times $t = 10^8$ without significantly spreading into any other site of the lattice (violet curve in Fig. 7). Slightly lowering β we observe that the excitation is trapped up to some time T_E which sensitively depends on β and changes by many orders of magnitude e.g. between 10^2 to 10^7 in the narrow interval $\beta \in (8.05, 8.9)$ for $E = 2$ (Fig. 7). For times $t > T_E$, an explosive and spatially asymmetric spreading is observed on a time scale of one

Bloch period T_B. The packet spreads in the direction of NMs with larger eigenvalues, which provide the possibility of resonant energy transfer from the single site excitation due to its positive nonlinear frequency shift δ. For about ten Bloch periods T_B the packet shows Bloch oscillations, which then quickly decohere. Finally the packet spreads incoherently and subdiffusively. The explosion time T_E is not monotonously changing with β, which indicates intermittency, i.e. the single site excitation can be closer or further away from some regular structures in phase space. That distance may in turn control the value of T_E. For $E = 2$ and $\beta = 8$ the packet spreads from scratch (blue curve in Fig. 7).

It is worth noting, that the border between regimes II and III can be approximated by a dimer model (an estimate from below). Indeed, a dimer model takes into account only one lattice site to the right from initially excited site (corresponding to the trapped state) and therefore describes the asymmetric energy transfer during the explosion. As for the disordered case, we observe that nonlinearity destroys integrability, introduces chaos, and ultimately leads to a subdiffusive spreading, so that the second moment grows as t^α with $\alpha < 1$. Our preliminary numerical studies showed that the exponent α is not universal and depends on the system parameters. The reason is that spreading of the wave packet takes place not anymore due to pure

incoherent transfer but becomes a complicated mixture of incoherent and coherent transfer processes. The interplay of these two mechanisms is a subject of our future studies.

2.2.3. *Single mode excitation*

A single mode excitation $\phi_\nu(t = 0) = \delta_{\nu,0}$ also exhibits the three different regimes of spreading. However, for small values of nonlinearity β a new intriguing feature of the short time dynamics follows [Krimer *et al.*, 2009]. Indeed, considering the resonant normal form one can conclude that a single mode excitation is the exact solution, so that no other NM is going to be excited. However, the full set of Eq. (28) will excite other NMs as well. These small perturbations may stay small or start to grow, depending on the stability of the single mode solution. Performing the linear stability analysis of the single mode excitation the stability intervals, which affect the short and long time dynamics, are obtained and observed upon variation of the DC bias strength. In particular, if the single mode excitation is launched within a stability window, we found that the wave packet is practically not spreading up to long time scales. However, a small change of the DC bias value E tunes the system into an instability window leading to a subdiffusive spreading on the accessible time scales, starting at short time scales.

2.3. *Nonlinear Aubry–André chains*

In quasiperiodic systems, the localized–delocalized transition discussed in Sec. 1.3 may be probed by a nonlinear interaction. Just as in Eqs. (15) and (27), this is done by adding a cubic term in the dynamics of Eq. (7):

$$i\frac{\partial \psi_l}{\partial t} = \zeta \cos(2\pi\alpha l) \cdot \psi_l - \psi_{l+1} - \psi_{l-1} + \beta|\psi_l|^2\psi_l. \tag{30}$$

Unlike the two previously discussed cases, the **linear** behavior of the second moment (introduced in Sec. 2.1.1) in the Aubry–André model was shown [Ketzmerick *et al.*, 1997; Hiramoto & Abe, 1988] to follow

$$m_2(t; \beta = 0) = \begin{cases} t^2 & \zeta < 2 \\ t^1 & \zeta = 2 \\ t^0 & \zeta > 2. \end{cases}$$

The nonlinear effect on the above packet spreading has garnered much attention in recent years, including experimental observations of the spreading in both Kerr photonics [Lahini *et al.*, 2009] and ultracold atomic clouds in optic traps [Ringot *et al.*, 2000; Deissler *et al.*, 2010]. In [Ng & Kottos, 2007], the critical case of $\zeta = 2$ was observed to have short transient behaviors dependent on the nonlinearity before asymptotically displaying an exponent similar to the linear behavior. In contrast, in [Larcher *et al.*, 2009] all ζ were investigated. Larcher *et al.* additionally incorporated a lattice phase shift, such that for Eq. (30), the potential becomes $\cos(2\pi\alpha l) \mapsto \cos(2\pi\alpha l + \theta)$. Starting from single-site excitations, they were able to develop the parametric space shown in Fig. 8. In this figure, three spreading regimes are found to be dictated by both the nonlinearity and lattice phase. The blue squares in the figure correspond to a lattice phase of zero, while the red circles correspond to a π phase. The first two regions display (I) strong self-trapping (similar to the $\delta > 2$ section of Fig. 3), and (II) subdiffusive spreading, but with discrete breather structures being seen. The main interest is within the localizing region (III), in which zero phases become self-trapped, and π phases become subdiffusive — these dependencies were hinted within [Johansson *et al.*, 1995]. Larcher *et al.* then go on to investigate the exponents in the moments and participations, much as
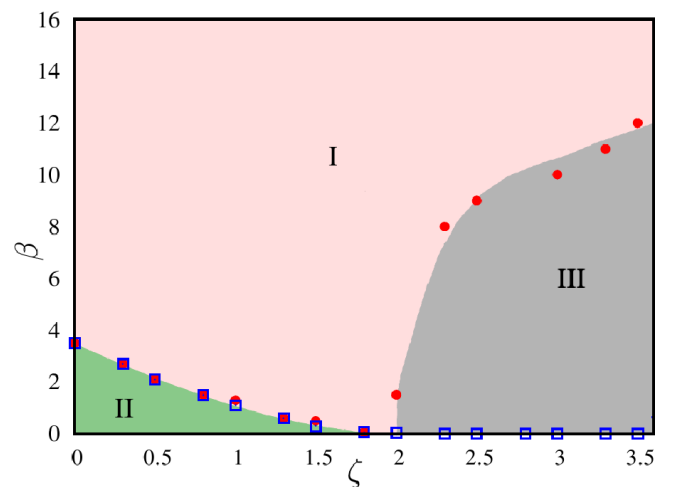

Fig. 8. Parametric space for nonlinear spreading in the Aubry–André model. The blue squares are for an initial excitation under a lattice phase $\theta = 0$, while the red circles are for an excitation under the phase $\theta = \pi$. The three regimes are discussed in detail within the text. Figure adapted from [Larcher *et al.*, 2009].

done for the DNLS and KG models in [Flach *et al.*, 2009]. Throughout, the spreading still remains sub-diffusive. Recent efforts have also seen experimental evidence to support such subdiffusive spreading [Lucioni *et al.*, 2010].

Almost all efforts in the Aubry–André model have been done for a single "realization" of the potential. However, to develop a universal description of spreading, moment averaging over realizations ought be considered — while there is no randomness in Eq. (30), one can perhaps introduce the idea of a "realization" by randomizing lattice phase θ, or perhaps over various incommensurate sets of α. As seen, particular attention needs to be paid in choosing the lattice phase. With the introduction of nonlinearity, the Aubry–André model remains a cornucopia of study.

2.4. *Quantum kicked rotor*

Realizations of Bose–Einstein condensation of dilute gases has opened new opportunities for experimental study of dynamical systems in the presence of many-body interactions. In the mean field approximation, these many-body interactions in the Bose–Einstein condensates are represented by adding a nonlinear term in the corresponding Schrödinger model equation [Benvenuto *et al.*, 1991]:

$$i\frac{\partial\psi}{\partial t} = -\frac{1}{2}\frac{\partial^2\psi}{\partial\theta^2} - \tilde{\beta}|\psi|^2\psi$$

$$+ k\cos(\theta)\psi\sum_{m=-\infty}^{+\infty}\delta(t-mT), \quad (31)$$

where the notation is the same as Eq. (10), except here with the new parameter $\tilde{\beta}$, which describes the nonlinear coupling.

The influence of nonlinearity on quantum localization in the nonlinear quantum kicked rotor can be studied by direct numerical simulation of the corresponding model, Eq. (31). The correct approach to approximate the evolution of the nonlinear Schrödinger equation is to evaluate the nonlinear term in the position representation [Benvenuto *et al.*, 1991]. Namely, for the numerical integration of Eq. (31), the lowest order split method can be used and the evolution operator $\hat{U}$ can be approximated by the time-ordered product of the evolution operators over small time steps T/L (with integer L) [Bandrauk & Shen, 1993]:

$$\hat{U}(T) = \exp(-ik\cos\hat{\theta})\prod_{j=1}^{L}\exp\left(-iT\frac{\hat{n}^2}{2L}\right)$$

$$\times \exp\left(i\tilde{\beta}\left(\frac{T}{L}\right)\left|\psi\left(\hat{\theta},\frac{jT}{L}\right)\right|^2\right). \quad (32)$$

In this model, the phase is acquired at each instant by the wavefunction, which involves all the Fourier components, and the phase factor of the nth Fourier component is $(\tilde{\beta}/2\pi)\sum_m\hat{\psi}^*_{m+n}\hat{\psi}_m$. The typical values of the number of steps per period are between $8\cdot10^5$ and $5\cdot10^6$. Therefore, this model is computationally quite expensive to study the effects of strong nonlinearities and the dynamics of the system over long time [Rebuzzini *et al.*, 2005].

Another much simpler model of the quantum kicked nonlinear rotor — which allows faster performance and more efficient numerical computations — was introduced by Shepelyansky [1993]. The dynamics of this model is given by the following map:

$$A_n(t+T) = \sum_m(-i)^{n-m}J_{n-m}(k)A_m(t)$$

$$\times \exp\left(-i\frac{1}{2}Tm^2 + i\beta|A_m|^2\right). \quad (33)$$

This map is almost the same as that without nonlinearity, Eq. (13). The only difference is that the change of the phase in the Fourier harmonics A_n between two kicks, now depends on the amplitude of the harmonics, $\Delta\phi_m = \beta|A_m|^2$. The parameter of the nonlinear coupling $\tilde{\beta}$ in the nonlinear Schrödinger equation (31) and the nonlinear parameter β in Eq. (33) are connected by the relation $\beta = T\tilde{\beta}/2\pi$.

Numerical results of the quantum kicked rotor model in the presence of nonlinearity show that the dynamics is affected by nonlinearity. In the resonant regime, where the parameter T is rational, the nonlinearity only affects the prefactor in the parabolic growth law, and the resonant regime persists [Rebuzzini *et al.*, 2005]. On the other hand, in the localized regime (irrational T) simulations demonstrate that nonlinearity destroys quantum localization. Namely, in the presence of strong enough nonlinearity, subdiffusive spreading is observed [Shepelyansky, 1993]. This effect of nonlinearity in the quantum kicked rotor is similar to those obtained in the models with disorder, as discussed in the previous sections. In the case of the

quantum kicked rotor, the role of disorder is played by the quasiperiodic sequence $\{(1/2)Tm^2\}$, which is obtained for irrational T. Replacement of this quasiperiodic sequence with a truly random one shows no change in the behavior of the system. This favors the expectations that the influence of nonlinearity can be described by the same theory developed in the context of the models with disorder. Preliminary results show that the compactness index ζ (see Sec. 2.1.1), which quantifies the wave packet sparsity, oscillates around values of 12 for the quantum kicked rotor model. This means that the wave packet spreads in a compact fashion. In addition, preliminary results indicate different subdiffusive spreading regimes with respect to the values of the coefficient of nonlinearity β and the strength of the kick k. We expect that these results can be explained by the existence of different spreading regimes of the wave packet, as in Sec. 2.1: the strong chaos, the weak chaos regime, and the crossover regime between. Currently, our recent efforts have been dedicated to establishing more clear and reliable results.

3. Outlook

A variety of linear wave equations support wave localization. Many of them were experimentally studied in recent times. The localization phenomenon relies on the phase coherence of waves. Therefore, destruction of phase coherence — dephasing — leads to a loss of wave localization. Nonlinear wave equations are in general nonintegrable, and therefore admit dynamical chaos. Dynamical chaos in turn leads to a loss of correlations — and therefore dephasing. Consequently wave propagation in nonlinear wave equations will generically lead to delocalization. We discussed a number of results on wave packet propagation which support this conclusion. Nonlinearity is the result of wave interactions, and a generic phenomenon in many physical realizations as well. Therefore, future experimental studies are expected to confirm these predictions.

Besides wave packet propagation, conductivity measurements are informative as well. In particular, the temperature dependence of the heat conductivity has been recently related directly to the properties of wave packet propagation [Flach *et al.*, 2011].

There are many future research directions the mind can take. Extensions to higher lattice dimensions are of interest. Two-dimensional lattices are numerically feasible, while three-dimensional cases need most probably the support of supercomputers. The interplay of nonlinearity with mobility edges and critical states can be expected to be intriguing as well. Quantizing the above nonlinear field equations remains a challenging enterprise.

References

Abrahams, E. [1979] "Scaling theory of localization: Absence of quantum diffusion in two dimensions," *Phys. Rev. Lett.* **42**, 673.

Albert, M. & Leboeuf, P. [2010] "Localization by bichromatic potentials versus Anderson localization," *Phys. Rev. A* **81**, 013614.

Albuquerque, E. & Cottam, M. [2003] "Theory of elementary excitations in quasiperiodic structures," *Phys. Rep.* **376**, 225.

Anderson, P. W. [1958] "Absence of diffusion in certain random lattices," *Phys. Rev.* **109**, 1492.

Anderson, B. & Kasevich, M. [1988] "Macroscopic quantum interference from atomic tunnel arrays," *Science* **282**, 1686.

Aubry, S. & André, G. [1980] "Analyticity breaking and Anderson localization in incommensurate lattices," *Ann. Israel Phys. Soc.* **3**, 133.

Aulbach, C., Wobst, A., Ingold, G., Hänggi, P. & Varga, I. [2004] "Phase-space visualization of a metal-insulator transition," *New J. Phys.* **6**, 70.

Bandrauk, A. D. & Shen, H. [1993] "Exponential split operator methods for solving coupled time-dependent Schrödinger equations," *The J. Chem. Phys.* **99**, 1185.

Basko, D. M. [2011] "Weak chaos in disordered nonlinear Schrödinger chain: Destruction of Anderson localization by Arnold diffusion," *Ann. Phys.* **326**, 1577.

Bayfield, J., Casati, G., Guarneri, I. & Sokol, D. [1989] "Localization of classically chaotic diffusion for hydrogen atoms in microwave fields," *Phys. Rev. Lett.* **63**, 364.

Benvenuto, F., Casati, G., Pikovsky, A. & Shepelyansky, D. [1991] "Manifestations of classical and quantum chaos in nonlinear wave propagation," *Phys. Rev. A* **44**, R3423.

Biddle, J., Wang, B., Priour, D. & Sarma, S. D. [2009] "Localization in one-dimensional incommensurate lattices beyond the Aubry–André model," *Phys. Rev. A* **80**, R021603.

Billy, J., Josse, V., Zuo, Z., Bernard, A., Hambrecht, B., Lugan, P., Clément, D., Sanchez-Palencia, L., Bouyer, P. & Aspect, A. [2008] "Direct observation of Anderson localization of matter waves in a controlled disorder," *Nature* **453**, 891.

Boers, D., Goedeke, B., Hinrichs, D. & Holthaus, M. [2007] "Mobility edges in bichromatic optical lattices," *Phys. Rev. A* **75**, 063404.

Casati, G., Chirikov, B., Izraelev, F. & Ford, J. [1979] "Stochastic behavior of a quantum pendulum under a periodic perturbation," *Stochastic Behavior in Classical and Quantum Hamiltonian Systems* (Springer-Verlag, Berlin/Heidelberg), pp. 334–352.

Chabé, J., Lemarié, G., Grémaud, B., Delande, D., Szriftgiser, P. & Garreau, J. [2008] "Experimental observation of the Anderson metal-insulator transition with atomic matter waves," *Phys. Rev. Lett.* **101**, 255702.

Chirikov, B. [1979] "A universal instability of many-dimensional oscillator systems," *Phys. Rep.* **52**, 263.

Datta, P. & Jayannavar, A. [1998] "Effect of nonlinearity on the dynamics of a particle in field-induced systems," *Phys. Rev. B* **58**, 8170.

Deissler, B., Zaccanti, M., Roati, G., D'Errico, C., Fattori, M., Modugno, M., Modugno, G. & Inguscio, M. [2010] "Delocalization of a disordered bosonic system by repulsive interactions," *Nature Phys.* **6**, 354.

Delande, D. & Gay, J. [1987] "Scars of symmetries in quantum chaos," *Phys. Rev. Lett.* **59**, 1809.

Diener, R., Georgakis, G., Zhong, J., Raizen, M. & Niu, Q. [2001] "Transition between extended and localized states in a one-dimensional incommensurate optical lattice," *Phys. Rev. A* **64**, 033416.

Edwards, J. T. & Thouless, D. J. [1972] "Numerical studies of localization in disordered systems," *J. Phys. C: Solid State Phys.* **5**, 807.

Fishman, S., Grempel, D. & Prange, R. [1982] "Chaos, quantum recurrences, and Anderson localization," *Phys. Rev. Lett.* **49**, 509.

Flach, S. & Willis, C. [1998] "Discrete breathers," *Phys. Rep.* **295**, 181.

Flach, S. & Gorbach, A. [2008] "Discrete breathers–advances in theory and applications," *Phys. Rep.* **467**, 1.

Flach, S., Krimer, D. O. & Skokos, C. [2009] "Universal spreading of wave packets in disordered nonlinear systems," *Phys. Rev. Lett.* **102**, 024101.

Flach, S. [2010] "Spreading of waves in nonlinear disordered media," *Chem. Phys.* **375**, 548.

Flach, S., Ivanchenko, M. & Li, N. [2011] "Thermal conductivity of nonlinear waves in disordered chains," arXiv:1101.4530v1 [cond-mat.stat-mech], to be published in *Pramana — J. Phys.*

Fukuyama, H., Bari, R. & Fogedby, H. [1973] "Tightly bound electrons in a uniform electric field," *Phys. Rev. B* **8**, 5579.

Griniasty, M. & Fishman, S. [1988] "Localization by pseudorandom potentials in one dimension," *Phys. Rev. Lett.* **60**, 1334.

Guidoni, L., Triché, C., Verkerk, P. & Grynberg, G. [1997] "Quasiperiodic optical lattices," *Phys. Rev. Lett.* **79**, 3363.

Gustavsson, M., Haller, E., Mark, M., Danzl, J., Rojas-Kopeinig, G. & Nägerl, H. [2008] "Control of interaction-induced dephasing of Bloch oscillations," *Phys. Rev. Lett.* **100**, 080404.

Harper, P. [1955a] "The general motion of conduction electrons in a uniform magnetic field, with application to the diamagnetism of metals," *Proc. Phys. Soc. Section A* **68**, 879.

Harper, P. [1955b] "Single band motion of conduction electrons in a uniform magnetic field," *Proc. Phys. Soc. Section A* **68**, 874.

Hiramoto, H. & Abe, S. [1988] "Dynamics of an electron in quasiperiodic systems. II. Harper's model," *J. Phys. Soc. Japan* **57**, 1365.

Hu, B., Li, B. & Tong, P. [2000] "Disturbance spreading in incommensurate and quasiperiodic systems," *Phys. Rev. B* **61**, 9414.

Hu, H., Strybulevych, A., Page, J. H., Skipetrov, S. E. & van Tiggelen, B. A. [2008] "Localization of ultrasound in a three-dimensional elastic network," *Nature Phys.* **4**, 945.

Hufnagel, L., Ketzmerick, R., Kottos, T. & Geisel, T. [2001] "Superballistic spreading of wave packets," *Phys. Rev. E* **64**, 012301.

Ingold, G., Wobst, A., Aulbach, C. & Hänggi, P. [2002] "Delocalization and Heisenberg's uncertainty relation," *The European Phys. J. B* **30**, 175.

Izrailev, F. [1990] "Simple models of quantum chaos: Spectrum and eigenfunctions," *Phys. Rep.* **196**, 299.

Johansson, M. & Riklund, R. [1991] "Self-dual model for one-dimensional incommensurate crystals including next-nearest-neighbor hopping, and its relation to the Hofstadter model," *Phys. Rev. B* **43**, 13468.

Johansson, M., Hörnquist, M. & Riklund, R. [1995] "Effects of nonlinearity on the time evolution of single-site localized states in periodic and aperiodic discrete systems," *Phys. Rev. B* **52**, 231.

Johansson, M. [2006] "Discrete nonlinear Schrödinger approximation of a mixed Klein–Gordon/Fermi–Pasta–Ulam chain: Modulational instability and a

statistical condition for creation of thermodynamic breathers," *Phys. D: Nonlin. Phenom.* **216**, 62.

Johansson, M., Kopidakis, G. & Aubry, S. [2010] "KAM tori in 1D random discrete nonlinear Schroedinger model?" *Europhys. Lett.* **91**, 50001.

Ketzmerick, R., Kruse, K., Kraut, S. & Geisel, T. [1997] "What determines the spreading of a wave packet?" *Phys. Rev. Lett.* **79**, 1959.

Kivshar, Y. & Peyrard, M. [1992] "Modulational instabilities in discrete lattices," *Phys. Rev. A* **46**, 3198.

Kivshar, Y. [1993] "Creation of nonlinear localized modes in discrete lattices," *Phys. Rev. E* **48**, 4132.

Kolovsky, A. R., Gómez, E. A. & Korsch, H. J. [2010] "Bose–Einstein condensates on tilted lattices: Coherent, chaotic, and subdiffusive dynamics," *Phys. Rev. A* **81**, 025603.

Kopidakis, G., Komineas, S., Flach, S. & Aubry, S. [2008] "Absence of wave packet diffusion in disordered nonlinear systems," *Phys. Rev. Lett.* **100**, 084103.

Kramer, B. & MacKinnon, A. [1993] "Localization: Theory and experiment," *Rep. Progr. Phys.* **56**, 1469.

Krimer, D. O., Khomeriki, R. & Flach, S. [2009] "Delocalization and spreading in a nonlinear Stark ladder," *Phys. Rev. E* **80**, 036201.

Krimer, D. O. & Flach, S. [2010] "Statistics of wave interactions in nonlinear disordered systems," *Phys. Rev. E* **82**, 046221.

Lahini, Y., Avidan, A., Pozzi, F., Sorel, M., Morandotti, R., Christodoulides, D. & Silberberg, Y. [2008] "Anderson localization and nonlinearity in one-dimensional disordered photonic lattices," *Phys. Rev. Lett.* **100**, 013906.

Lahini, Y., Pugatch, R., Pozzi, F., Sorel, M., Morandotti, R., Davidson, N. & Silberberg, Y. [2009] "Observation of a localization transition in quasiperiodic photonic lattices," *Phys. Rev. Lett.* **103**, 013901.

Landau, L. [1932] "On the theory of transfer of energy at collisions II," *Physikalische Zeitschrift der Sowjetunion* **2**, 46.

Laptyeva, T. V., Bodyfelt, J. D., Krimer, D. O., Skokos, C. & Flach, S. [2010] "The crossover from strong to weak chaos for nonlinear waves in disordered systems," *Europhys. Lett.* **91**, 30001.

Larcher, M., Dalfovo, F. & Modugno, M. [2009] "Effects of interaction on the diffusion of atomic matter waves in one-dimensional quasiperiodic potentials," *Phys. Rev. A* **80**, 053606.

Levine, D. & Steinhardt, P. [1984] "Quasicrystals: A new class of ordered structures," *Phys. Rev. Lett.* **53**, 2477.

Li, S., Satija, I., Clark, C. & Rey, A. [2010] "Exploring complex phenomena using ultracold atoms in bichromatic lattices," *Phys. Rev. E* **82**, 016217.

Liu, J., Fu, L., Ou, B., Chen, S., Choi, D., Wu, B. & Niu, Q. [2002] "Theory of nonlinear Landau–Zener tunneling," *Phys. Rev. A* **66**, 023404.

Lucioni, E., Deissler, B., Tanzi, L., Roati, G., Modugno, M., Zaccanti, M., Inguscio, M. & Modugno, G. [2010] "Observation of subdiffusion of a disordered interacting system," arXiv:1011.2362v1 [cond-mat.dis-nn].

Maciá, E. & Domínguez-Adame, F. [2000] *Electrons, Phonons and Excitons in Low Dimensional Aperiodic Systems*, 1st edition (Editorial Complutense, Madrid).

Modugno, G. [2010] "Anderson localization in Bose–Einstein condensates," *Rep. Progr. Phys.* **73**, 102401.

Modugno, M. [2009] "Exponential localization in one-dimensional quasi-periodic optical lattices," *New J. Phys.* **11**, 033023.

Molina, M. [1998] "Transport of localized and extended excitations in a nonlinear Anderson model," *Phys. Rev. B* **58**, 12547.

Moore, F., Robinson, J., Bharucha, C., Sundaram, B. & Raizen, M. [1995] "Atom optics realization of the quantum δ-kicked rotor," *Phys. Rev. Lett.* **75**, 4598.

Morandotti, R., Peschel, U., Aitchison, J., Eisenberg, H. & Silberberg, Y. [1999] "Experimental observation of linear and nonlinear optical Bloch oscillations," *Phys. Rev. Lett.* **83**, 4756.

Morsch, O., Müller, J., Cristiani, M., Ciampini, D. & Arimondo, E. [2001] "Bloch oscillations and mean-field effects of Bose–Einstein condensates in 1D optical lattices," *Phys. Rev. Lett.* **87**, 140402.

Mulansky, M., Ahnert, K., Pikovsky, A. & Shepelyansky, D. L. [2009] "Dynamical thermalization of disordered nonlinear lattices," *Phys. Rev. E* **80**, 056212.

Ng, G. & Kottos, T. [2007] "Wavepacket dynamics of the nonlinear Harper model," *Phys. Rev. B* **75**, 205120.

Pertsch, T., Dannberg, P., Elflein, W., Bräuer, A. & Lederer, F. [1999] "Optical Bloch oscillations in temperature tuned waveguide arrays," *Phys. Rev. Lett.* **83**, 4752.

Pikovsky, A. & Shepelyansky, D. [2008] "Destruction of Anderson localization by a weak nonlinearity," *Phys. Rev. Lett.* **100**, 094101.

Rebuzzini, L., Wimberger, S. & Artuso, R. [2005] "Delocalized and resonant quantum transport in nonlinear generalizations of the kicked rotor model," *Phys. Rev. E* **71**, 036220.

Ringot, J., Szriftgiser, P., Garreau, J. & Delande, D. [2000] "Experimental evidence of dynamical localization and delocalization in a quasiperiodic driven system," *Phys. Rev. Lett.* **85**, 2741.

Roati, G., D'Errico, C., Fallani, L., Fattori, M., Fort, C., Zaccanti, M., Modugno, G., Modugno, M. & Inguscio, M. [2008] "Anderson localization of a non-interacting Bose–Einstein condensate," *Nature* **453**, 895.

Sarma, S. D., He, S. & Xie, X. [1988] "Mobility edge in a model one-dimensional potential," *Phys. Rev. Lett.* **61**, 2144.

Schwartz, T., Bartal, G., Fishman, S. & Segev, M. [2007] "Transport and Anderson localization in

disordered two-dimensional photonic lattices," *Nature* **446**, 52.

Shepelyansky, D. [1993] "Delocalization of quantum chaos by weak nonlinearity," *Phys. Rev. Lett.* **70**, 1787.

Skokos, C., Krimer, D. O., Komineas, S. & Flach, S. [2009] "Delocalization of wave packets in disordered nonlinear chains," *Phys. Rev. E* **79**, 056211.

Skokos, C. & Flach, S. [2010] "Spreading of wave packets in disordered systems with tunable nonlinearity," *Phys. Rev. E* **82**, 016208.

Soukoulis, C. & Economou, E. [1982] "Localization in one-dimensional lattices in the presence of incommensurate potentials," *Phys. Rev. Lett.* **48**, 1043.

Störzer, M., Gross, P., Aegerter, C. & Maret, G. [2006] "Observation of the critical regime near Anderson localization of light," *Phys. Rev. Lett.* **96**, 063904.

Trebin, H. (ed.) [2003] *Quasicrystals*: *Structure and Physical Properties* (Wiley-VCH, Weinheim, Cambridge).

Tsu, R. [1993] "Field induced localization in superlattices," *Semiconductor Interfaces, Microstructures and Devices*: *Properties and Applications*, ed. Feng, Z.

(Institute of Physics Pub., Bristol; Philadelphia), pp. 3–19.

Varga, I., Pipek, J. & Vasvári, B. [1992] "Power-law localization at the metal-insulator transition by a quasiperiodic potential in one dimension," *Phys. Rev. B* **46**, 4978.

Vekilov, Y. K. & Chernikov, M. A. [2010] "Quasicrystals," *Physics-Uspekhi* **53**, 537.

Veksler, H., Krivolapov, Y. & Fishman, S. [2009] "Spreading for the generalized nonlinear Schrödinger equation with disorder," *Phys. Rev. E* **80**, 037201.

Wannier, G. [1960] "Wave functions and effective Hamiltonian for Bloch electrons in an electric field," *Phys. Rev.* **117**, 432.

Wiersma, D. S., Bartolini, P., Lagendijk, A. & Righini, R. [1997] "Localization of light in a disordered medium," *Nature* **390**, 671–673.

Zener, C. [1932] "Non-adiabatic crossing of energy levels," *Proc. Roy. Soc. London. Series A, Containing Papers of a Mathematical and Physical Character* **137**, 696.